Domain decomposition methods combining surface equivalence principle and macro basis functions

Document status and date:
Published: 01/01/2010

Document Version:
Publisher's PDF, also known as Version of Record (includes final page, issue and volume numbers)

Please check the document version of this publication:

• A submitted manuscript is the version of the article upon submission and before peer-review. There can be important differences between the submitted version and the official published version of record. People interested in the research are advised to contact the author for the final version of the publication, or visit the DOI to the publisher's website.
• The final author version and the galley proof are versions of the publication after peer review.
• The final published version features the final layout of the paper including the volume, issue and page numbers.

Link to publication

Download date: 16. Nov. 2023

Domain Decomposition Methods Combining Surface Equivalence Principle and Macro Basis Functions

Pasi Ylä-Oijala[1], Vito Lancellotti[2], Bastiaan P. de Hon[2], and Seppo Järvenpää[1]

[1]Aalto University, Department of Radio Science and Engineering
P.O. Box 13000, FI-00076 AALTO, Finland, pasi.yla-oijala@tkk.fi

[2]Department of Electrical Engineering, Eindhoven University of Technology
P.O. Box 513, 5600 MB Eindhoven, The Netherlands, V.Lancellotti@tue.nl

Abstract – The basics of two domain decomposition methods based on the surface equivalence principle and the method of moments, namely, the surface tangential equivalence principle (TEPA) and the linear embedding via Green's operators (LEGO), are outlined to solve electromagnetic scattering problems. In order to efficiently solve large problems, the methods are combined with the characteristic basis function method and the eigencurrent expansion method. Numerical examples demonstrate that the developed hybrid techniques lead to a significant reduction on the number of degrees of freedom and the size of the matrix equation to be solved.

Index Terms – Domain decomposition methods, electromagnetic scattering, method of moments, multi-scale problems, surface integral equations.

I. INTRODUCTION

Electromagnetic (EM) scattering by large and complex structures, such as EM band gaps, frequency selective surfaces, metamaterials, antenna arrays, etc. have received a lot of interest lately. In the conventional integral equation and finite element approaches, the structure is first divided into simple elements and then the unknown quantities, currents or fields, are expanded with basis functions defined on these elements. As the size of the structure gets large, the number of elements required to sufficiently model the unknown and the structure details increases, eventually leading to the problem of solving huge, possibly very ill-conditioned, linear systems. This may be a very challenging task even with the most powerful computers and efficient fast algorithms.

Domain decomposition methods (DDM) have been successfully used to solve many complex multi-scale EM problems, in particular, in the context of the finite element method, see e.g. [1] and [2]. The basic idea in a DDM is to divide a large and complex problem into smaller and simpler subproblems that can be solved independently. This essentially isolates the solution of one region from another and in many cases significantly improves the matrix conditioning. The other benefits of DDMs include, for example, the inherent aptitude for parallelization and for usage in combination with hybrid methods.

In this paper, we discuss two DDM approaches based on the surface equivalence (Huygens) principle and the method of moments (MoM) to solve large and complex EM problems. The algorithms are the surface tangential equivalence principle algorithm (TEPA) [3] and the linear embedding via Green's operators (LEGO) [4]. TEPA is a modification of the equivalence principle algorithm [5–7] and LEGO is the full 3-D extension of the procedure presented in [8].

In many cases, these algorithms can lead to savings on the number of unknowns and improvements on the condition number of the matrix compared to the traditional MoM formulations. However, the methods still produce dense matrix equations and the computational cost increases with the same rate as in the conventional formulations. Hence, the methods can become too expensive for large scale problems. In order to further reduce the number of unknowns and the solution time, TEPA and LEGO are combined with the characteristic basis function method (CBFM) [9–13] and the eigencurrent expansion method (EEM) [4], respectively.

II. INTEGRAL EQUATIONS

Let us consider time-harmonic electromagnetic (EM) scattering by a large number of arbitrarily shaped objects D_p, $p = 1, \ldots, P$, in a homogeneous background D_0. The objects can be either perfect electric conductors (PEC) or homogeneous dielectric, as well as their combinations. For simplicity, assume that the objects are disjoint.

Let S_p denote the surface of D_p. The scattered EM fields $\boldsymbol{E}_p^s$ and $\boldsymbol{H}_p^s$ due to D_p can be expressed at point $\boldsymbol{r}$ in D_0 as

$$
\begin{bmatrix} \boldsymbol{E}_{0p}^s \\ \boldsymbol{H}_{0p}^s \end{bmatrix} = \begin{bmatrix} \eta_0 \, \boldsymbol{\mathcal{L}}_{0p}^{(0)} & -\boldsymbol{\mathcal{K}}_{0p}^{(0)} \\ \boldsymbol{\mathcal{K}}_{0p}^{(0)} & \frac{1}{\eta_0} \boldsymbol{\mathcal{L}}_{0p}^{(0)} \end{bmatrix} \begin{bmatrix} \boldsymbol{J}_p \\ \boldsymbol{M}_p \end{bmatrix}. \quad (1)
$$

Here $\eta_0 = \sqrt{\mu_0/\varepsilon_0}$ is the wave impedance of D_0, $\boldsymbol{J}_p = \boldsymbol{n}_p \times \boldsymbol{H}_p$ and $\boldsymbol{M}_p = -\boldsymbol{n}_p \times \boldsymbol{E}_p$ are the equivalent electric and magnetic current densities on S_p with the unit normal vector $\boldsymbol{n}_p$ pointing into D_0. The surface integral operators $\boldsymbol{\mathcal{L}}_{qp}^{(d)}$ and $\boldsymbol{\mathcal{K}}_{qp}^{(d)}$ are defined as

$$
\begin{aligned}
\boldsymbol{\mathcal{L}}_{qp}^{(d)}(\boldsymbol{F})(\boldsymbol{r}) &= \frac{-1}{ik_q} \nabla \int_{S_p} G_d(\boldsymbol{r}, \boldsymbol{r}') \nabla_s' \cdot \boldsymbol{F}(\boldsymbol{r}') \, dS' \\
&\quad + ik_q \int_{S_p} G_d(\boldsymbol{r}, \boldsymbol{r}') \boldsymbol{F}(\boldsymbol{r}') \, dS' \\
&\quad + \frac{\delta_{S_p} \boldsymbol{n}(\boldsymbol{r})}{2ik_q} \nabla_s \cdot \boldsymbol{F}(\boldsymbol{r}), \quad (2)
\end{aligned}
$$

$$
\begin{aligned}
\boldsymbol{\mathcal{K}}_{qp}^{(d)}(\boldsymbol{F})(\boldsymbol{r}) &= \nabla \times \int_{S_p} G_d(\boldsymbol{r}, \boldsymbol{r}') \boldsymbol{F}(\boldsymbol{r}') \, dS' \\
&\quad - \frac{\delta_{S_p}}{2} \boldsymbol{n}(\boldsymbol{r}) \times \boldsymbol{F}(\boldsymbol{r}), \quad (3)
\end{aligned}
$$

where $k_q = \omega \sqrt{\varepsilon_q \mu_q}$ is the wavenumber of D_q, $\boldsymbol{r}' \in S_p$, $\boldsymbol{r} \in D_q$ and

$$
G_d(\boldsymbol{r}, \boldsymbol{r}') = \frac{e^{ik_d |\boldsymbol{r} - \boldsymbol{r}'|}}{4\pi |\boldsymbol{r} - \boldsymbol{r}'|}, \quad (4)
$$

is the homogeneous space Green's function of D_d with the wavenumber of D_d. In addition, $\boldsymbol{F}$ is either $\boldsymbol{M}_p$ or $\boldsymbol{J}_p$, and

$$
\delta_{S_p} = \begin{cases} 1 & \text{if } \boldsymbol{r} \in S_p, \\ 0 & \text{otherwise.} \end{cases} \quad (5)
$$

By expressing the fields separately in each non-PEC domain with (1) and by applying the EM boundary conditions on the interfaces and surfaces gives a set of surface integral equations that can be solved numerically with the MoM. The problem is that if the number of the objects is large and/or the structures are complicated, this traditional surface integral equation formulation leads to a large and ill-conditioned dense matrix equation which is difficult to solve. In the following sections the scattering problem is reformulated using domain decomposition methods.

III. DOMAIN DECOMPOSITION

The basic idea of the formulation applied in this paper is to reformulate the original scattering problem as a new equivalent problem with generalized scattering and translation operators. First, the objects (scatterers) are divided into groups. The groups may consist of one or more objects and are enclosed by virtual equivalence surfaces R_l, $l = 1, \ldots, L$. The domains enclosed by surfaces R_l are called bricks. Next, we define the scattering and translation operators of the bricks. The grouping, bricks, and the scattering and translation operators are illustrated in Figure 1.

A. Scattering operators

Let us first consider the EM problem consisting of a single brick only. The brick embeds a structure which, being illuminated by an incident field $\boldsymbol{F}^i = [\boldsymbol{E}^i, \boldsymbol{H}^i]^T$, develops induced (secondary) sources that radiate the scattered field $\boldsymbol{F}^s = [\boldsymbol{E}^s, \boldsymbol{H}^s]^T$. That scattered field remains the same if we replace the actual sources on the structure inside the brick with equivalent (secondary) sources $\boldsymbol{J}_l^s$ and $\boldsymbol{M}_l^s$ on the surface of the brick. Formally, this can be expressed via a generalized scattering operator $\boldsymbol{\mathcal{S}}_{ll}$ of the brick l as a mapping from the incident currents $\boldsymbol{U}_l^i$ onto the secondary currents $\boldsymbol{U}_l^s$

$$
\boldsymbol{U}_l^s = \boldsymbol{\mathcal{S}}_{ll} \boldsymbol{U}_l^i, \qquad \boldsymbol{U}_l^{s/i} = \left[\boldsymbol{J}_l^{s/i}, \boldsymbol{M}_l^{s/i} \right]^T. \quad (6)
$$

The scattering operator is defined via the use of the surface equivalence principle (1) as a product of four surface integral operators, as follows

$$
\boldsymbol{\mathcal{S}}_{ll} = \left(\boldsymbol{\mathcal{P}}_{ll}^{(0)} \right)^{-1} \boldsymbol{\mathcal{P}}_{lp}^{(0)} \left(\boldsymbol{\mathcal{P}}_{pp}^{(0)} \right)^{-1} \boldsymbol{\mathcal{P}}_{pl}^{(0)}, \quad (7)
$$

where the operators $\left(\boldsymbol{\mathcal{P}}_{ll}^{(0)} \right)^{-1}$, $\boldsymbol{\mathcal{P}}_{lp}^{(0)}$, $\boldsymbol{\mathcal{P}}_{pl}^{(0)}$ and $\boldsymbol{\mathcal{P}}_{pp}^{-1}$ are called the self-propagator, inside-out propagator, and outside-in propagator and the current solver, respectively. Here, the first lower index indicates
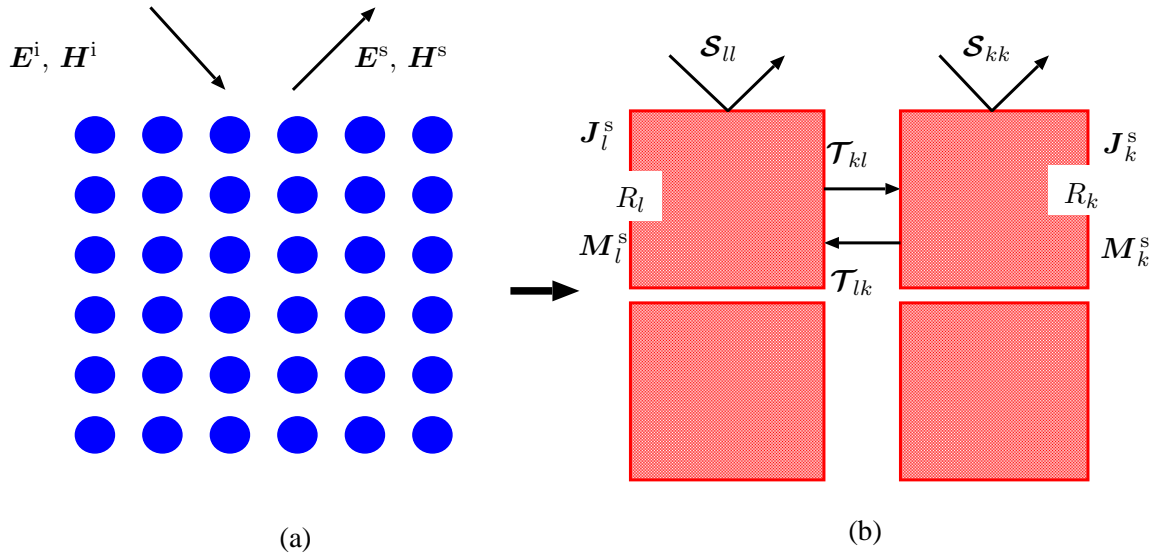
Fig. 1. Reformulation of a scattering problem. Left: original scattering problem. Right: reformulated problem with the scattering and translation operators and new unknowns.

the surface of the observation point, the second one indicates the surface of the source point, and the upper index indicates the domain whose Green's function is used in (1). The actual form of the operators depends on both the nature of the object and the adopted formulation [3, 4]. For example, in the case of homogeneous penetrable objects modeled with the PMCHWT (Poggio-Miller-Chang-Harrington-Wu-Tsai) formulation the propagators have the following expressions

$$\boldsymbol{\mathcal{P}}_{ij}^{(d)} = \begin{bmatrix} \eta^{(d)}\boldsymbol{\mathcal{L}}_{ij}^{(d)} & -\boldsymbol{\mathcal{K}}_{ij}^{(d)} \\ \boldsymbol{\mathcal{K}}_{ij}^{(d)} & \frac{1}{\eta^{(d)}}\boldsymbol{\mathcal{L}}_{ij}^{(d)} \end{bmatrix}_{\tan}, \qquad (8)$$

where $i, j = l, k$, or p and tan denotes the tangential component. Also the current solver, $\boldsymbol{\mathcal{P}}_{pp}$, can be expressed with the same propagation operators as

$$\boldsymbol{\mathcal{P}}_{pp} = \boldsymbol{\mathcal{P}}_{pp}^{(0)} + \boldsymbol{\mathcal{P}}_{pp}^{(p)}, \qquad (9)$$

where 0 stands for the background and p for the object. For the PEC objects modeled with the EFIE (electric field integral equation), the inside-out and outside-in propagators have to be modified as

$$\boldsymbol{\mathcal{P}}_{lp}^{(0)} = \begin{bmatrix} \eta_0\boldsymbol{\mathcal{L}}_{lp}^{(0)} & \boldsymbol{\mathcal{K}}_{lp}^{(0)} \end{bmatrix}_{\tan}^{T}, \qquad (10)$$

$$\boldsymbol{\mathcal{P}}_{pl}^{(0)} = \begin{bmatrix} \eta_0\boldsymbol{\mathcal{L}}_{pl}^{(0)} & -\boldsymbol{\mathcal{K}}_{pl}^{(0)} \end{bmatrix}_{\tan}, \qquad (11)$$

and $\boldsymbol{\mathcal{P}}_{pp} = \eta_0(\boldsymbol{\mathcal{L}}_{pp}^{(0)})_{\tan}$ is the EFIE operator on S_p.

B. Translation operators

Let us next consider the EM problem consisting of two separate bricks l and k with surfaces R_l and R_k. The direct scattering from the bricks is described with the scattering operators $\boldsymbol{\mathcal{S}}_{ll}$ and $\boldsymbol{\mathcal{S}}_{kk}$ as in (6). The scattering operators, however, do not model the interactions (multiple scattering) between the bricks. The multiple scattering between the bricks are particularly important if the bricks are close to each other.

The field scattered by brick k, i.e., the field due to secondary current $\boldsymbol{U}_k^s = \boldsymbol{\mathcal{S}}_{kk}\boldsymbol{U}_k^i$, produces new fields to R_l. These fields can be interpreted as incident currents on R_l and can be expressed via a translation operator $\boldsymbol{\mathcal{T}}_{lk}$, $l \neq k$, as

$$\boldsymbol{U}_{lk}^i = \boldsymbol{\mathcal{T}}_{lk}\boldsymbol{\mathcal{S}}_{kk}\boldsymbol{U}_k^i. \qquad (12)$$

The translation operator can be defined using the same self and outside-in propagators as the scattering operator

$$\boldsymbol{\mathcal{T}}_{lk} = \left(\boldsymbol{\mathcal{P}}_{ll}^{(0)}\right)^{-1}\boldsymbol{\mathcal{P}}_{lk}^{(0)}, \qquad (13)$$

Note that the form of the translation operators do not depend on the nature of the scatterers nor the applied integral equation formulation. The secondary current on R_l is now given by

$$\begin{aligned} \boldsymbol{U}_l^s &= \boldsymbol{\mathcal{S}}_{ll}\boldsymbol{U}_l^i + \boldsymbol{\mathcal{S}}_{ll}\boldsymbol{\mathcal{T}}_{lk}\boldsymbol{\mathcal{S}}_{kk}\boldsymbol{U}_k^i \\ &= \boldsymbol{\mathcal{S}}_{ll}\left(\boldsymbol{U}_l^i + \boldsymbol{\mathcal{T}}_{lk}\boldsymbol{U}_k^s\right). \end{aligned} \qquad (14)$$
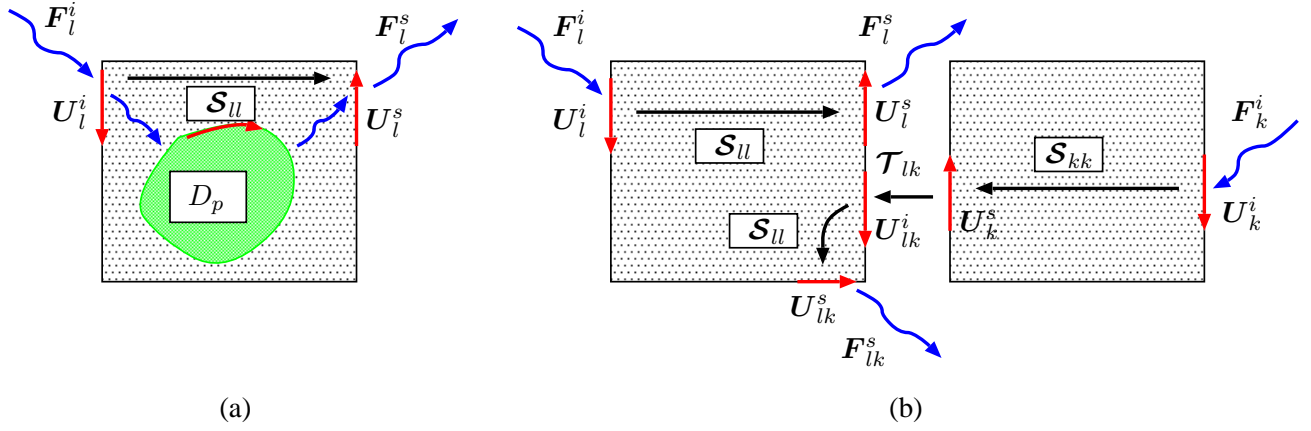
Fig. 2. Scattering and translation operators seen by the brick l: (a) single brick, (b) two bricks.

The procedure can be generalized for L bricks as

$$U_l^s = \mathcal{S}_{ll} \left(U_l^i + \sum_{k=1,k\neq l}^{L} \mathcal{T}_{lk} U_k^s \right), \qquad (15)$$

$l = 1, \ldots, L$. This can be expressed by a matrix

$$\begin{bmatrix} \mathcal{I} & -\mathcal{S}_{11}\mathcal{T}_{12} & \ldots & -\mathcal{S}_{11}\mathcal{T}_{1L} \\ -\mathcal{S}_{22}\mathcal{T}_{21} & \mathcal{I} & \ldots & -\mathcal{S}_{22}\mathcal{T}_{2L} \\ \vdots & & \ddots & \vdots \\ -\mathcal{S}_{LL}\mathcal{T}_{L1} & \ldots & & \mathcal{I} \end{bmatrix} \begin{bmatrix} U_1^s \\ U_2^s \\ \vdots \\ U_L^s \end{bmatrix}$$
$$= \begin{bmatrix} \mathcal{S}_{11}U_1^i \\ \mathcal{S}_{22}U_2^i \\ \vdots \\ \mathcal{S}_{LL}U_L^i \end{bmatrix}, \qquad (16)$$

where $\mathcal{I}$ is the identity operator. Next, we reformulate matrix (16) by solving equations (15) with respect to U_l^i

$$U_l^i = \mathcal{S}_{ll}^{-1} U_l^s - \sum_{k=1,k\neq l}^{L} \mathcal{T}_{lk} U_k^s, \qquad (17)$$

giving

$$\begin{bmatrix} \mathcal{S}_{11}^{-1} & -\mathcal{T}_{12} & \ldots & -\mathcal{T}_{1L} \\ -\mathcal{T}_{21} & \mathcal{S}_{22}^{-1} & \ldots & -\mathcal{T}_{2L} \\ \vdots & & \ddots & \vdots \\ -\mathcal{T}_{L1} & \ldots & & \mathcal{S}_{LL}^{-1} \end{bmatrix} \begin{bmatrix} U_1^s \\ U_2^s \\ \vdots \\ U_L^s \end{bmatrix} = \begin{bmatrix} U_1^i \\ U_2^i \\ \vdots \\ U_L^i \end{bmatrix}. \qquad (18)$$

The matrix on the left hand side of (18) can be interpreted as a total inverse scattering operator [4].

The benefit of (18) over (16) is that only the diagonal entries, $\mathcal{S}_{ll}^{-1}$, convey information about the objects comprising the structure. In contrast, the off-diagonal entries, $-\mathcal{T}_{lk}$, which tell how the bricks interact, do not depend on the bricks content, but solely on their relative position in the structure. This means that if, we allow for a change either in the EM properties or in the shape of the objects within each brick, only the diagonal terms $\mathcal{S}_{ll}^{-1}$ have to be re-computed.

The tangential equivalence principle algorithm (TEPA) [3] is based on (16) and the linear embedding with Green's operators (LEGO) [4] uses (18). For more details we refer to [3] and [4].

IV. NUMERICAL DISCRETIZATION

In the previous section, the original scattering problem was reformulated as a new problem by utilizing the generalized scattering and translation operators and the unknowns are the secondary equivalent surface current densities on the surfaces of the bricks. The next step is to convert the operator equations into discretized matrix equations. We will apply standard MoM with Galerkin's method and Rao-Wilton-Glisson (RWG) functions defined on planar triangular elements.

First, the unknown secondary currents on the surfaces of the bricks are expanded with the RWG functions f_l as

$$J_l^s \approx \sum_{n=1}^{N^l} \alpha_n^{(l)} f_l, \quad \text{and} \quad M_l^s \approx \sum_{n=1}^{N^l} \beta_n^{(l)} f_l. \quad (19)$$

Then these approximations are substituted into the equations, i.e., either to (16) or to (18). Next, we discretize the scattering and translation operators, $\mathcal{S}_{ll}$ and $\mathcal{T}_{lk}$. Since these operators are defined by the standard surface integral operators $\mathcal{L}$ and $\mathcal{K}$, they are discretized similarly as the traditional surface integral formulations. As a result, we may write (6) and (13) as

$$[S_{ll}] = [P_{ll}^{(0)}]^{-1} [P_{lp}^{(0)}] [P_{pp}]^{-1} [P_{pl}^{(0)}], \qquad (20)$$

and

$$[T_{lk}] = [P_{ll}^{(0)}]^{-1} [P_{lk}^{(0)}], \quad k \neq l, \qquad (21)$$

where the matrices on the right hand sides denote the matrices due to the propagators and the current solver.

The right hand side of equation (16) is considered as follows. Let b_l^E and b_l^H denote the usual excitation vectors due to the incident electric and magnetic fields on R_l tested with the RWG functions. Then, the incident currents on R_l are replaced with

$$[U_l^i] = [P_{ll}^{(0)}]^{-1} [b_l^E, b_l^H]^T. \qquad (22)$$

Once all operators are discretized and the continuous operator equations are converted into a matrix equation, the matrix equation can be solved either with a direct or an iterative method. This gives us the coefficients of the secondary currents on the surfaces of the bricks. Thereafter, the scattered fields can be calculated outside the bricks using the surface integral representations (1).

V. MACRO BASIS FUNCTIONS

In many cases, the procedure introduced above can lead to savings on the number of unknowns and improvements on the condition number of the matrix compared to the traditional MoM formulations. However, the method still produces dense matrix equation and the computational cost increases with the same rate as in the conventional MoM formulation. To efficiently solve large scale problems, next we discuss two macro basis function methods, to further reduce the number of degrees of freedom (DoF).

A. Characteristic basis functions

Consider first, the characteristic basis function method (CBFM) [9–13]. CBFM is a generic technique to reduce the size of the discretized matrix equation. In CBFM, the object (or objects) are divided into

groups (blocks). The matrix equation for L groups can be expressed as

$$\begin{bmatrix} A_{11} & \cdots & A_{1L} \\ \vdots & \ddots & \vdots \\ A_{L1} & \cdots & A_{LL} \end{bmatrix} \begin{bmatrix} U_1 \\ \vdots \\ U_L \end{bmatrix} = \begin{bmatrix} b_1 \\ \vdots \\ b_L \end{bmatrix}, \qquad (23)$$

where A_{lk} denotes a matrix block due to the interaction of the lth and kth group, U_l are the unknowns of the lth group and b_l is the excitation vector due to the lth group. Assume next that the bricks and the CBFM groups coincide.

The CBFs of the groups can be determined with alternative ways. In [9], so called primary and secondary CBFs of the blocks, $f_l^{(l)}$ and $f_k^{(l)}$, are defined as follows

$$f_l^{(l)} = A_{ll}^{(-1)} b_l, \qquad (24)$$

$$f_k^{(l)} = A_{ll}^{(-1)} \left(-A_{lk} f_k^{(k)} \right), \quad l \neq k, \qquad (25)$$

for all $l, k = 1, \ldots, L$. By applying this to (16) gives

$$f_l^{(l)} = \mathcal{S}_{ll} U_l^{\text{inc}}, \qquad (26)$$

$$f_k^{(l)} = -\mathcal{S}_{ll} \mathcal{T}_{lk} f_k^{(k)}, \quad l \neq k. \qquad (27)$$

Hence, the CBFs for system (16) can be obtained without need to invert any matrix.

Later in [10], an alternative method to find the CBFs was presented. In this approach each group is illuminated with a sufficiently large number of planewaves incident from different angles. The most significant planewave based CBFs

$$f_k^{(l)}, l = 1, \ldots, L, k = 1, \ldots, \tilde{N}^{PW}, \qquad (28)$$

are found via the use of SVD [10] and used as CBFs of the groups, i.e., the bricks.

In both approaches, the unknowns of each brick are expanded with these new basis functions, CBFs, as

$$U_l^s = \sum_k \alpha_k^{(l)} f_k^{(l)}, \quad \text{for all } l = 1, \ldots, L. \qquad (29)$$

Once the coefficients of the CBFs are found, the coefficients of the original subdomain basis functions can be obtained from (29). These methods are denoted by TEPA-CBFM and TEPA-CBFM-pw, respectively, since they are based on the TEPA formulation of [3] and equation (16).

Table 1: Geometrical data and the numbers triangles and edges for a single dipole and brick: the second column gives the data for the first example (single cross dipole), and the last two for the second one (double cross dipole)

	Single dipole	Double dipole (first case)	Double dipole (second case)
Dipole arm width	2 mm	2 mm	2 mm
Dipole arm length	12 mm	12 mm	12 mm
Vertical distance between dipoles	–	2 mm	2mm
Triangles on dipole	88	420	420
Edges on dipole	108	552	552
Brick shorter edge	5 mm	4 mm	4 mm
Brick longer edge	16 mm	16 mm	20 mm
Distance between brick centers	32 mm	22.5 mm	22.5 mm
Triangles on brick	256	256	360
Edges on brick	384	384	540

B. Eigencurrent expansions

Next, we consider another technique to find the macro basis functions of the bricks. The method is called the eigencurrent expansion method (EEM) and used with the LEGO in [4]. The EEM uses the eigenfunctions of $\mathcal{S}_{ll}$, called eigencurrents, to expand the unknowns on the surfaces of the bricks. The resulting method is denoted by LEGO-EEM.

We form a basis out of the eigenvectors of $[S_{ll}]$ and we practically implement the EEM as a basis change from the set of RWG functions [4]. We separate the eigencurrents into two groups: coupled and uncoupled. The coupled eigencurrents, associated with the larger, lower-order eigenvalues of $[S_{ll}]$, substantially depart from the true eigencurrents of $[S]$, the total scattering matrix, and contribute to the multiple scattering occurring among the bricks. By contrast, the uncoupled eigencurrents, associated with the smaller, higher-order eigenvalues of $[S_{ll}]$, represent better and better approximations to the true eigencurrents of $[S]$, and do not interact with one another.

These observations enabled us to reduce the system matrix $[S]^{-1}$ (in the basis of the eigencurrents) to block-diagonal form with just two blocks. In particular, the block arising from the interaction of the coupled eigencurrents is usually far smaller than the whole system matrix, so it can be easily stored and inverted with direct methods. The other block, possibly huge, is just diagonal, hence it can effortlessly be stored and (formally) inverted. The order reduction we have just described is actually a consequence of two concurring, though independent, facts: i) the

eigenvalues of $[S_{ll}]$ decrease; ii) the entries of $[T_{lk}]$ become smaller and smaller when the distance between bricks l and k increases [14].

VI. NUMERICAL RESULTS

Next, the developed methods are verified with numerical examples and their properties are investigated.

As a first numerical example, we consider the scattering by a 5×5 array of thin PEC cross dipoles arranged in a regular lattice parallel to the xy plane. The dipoles are embedded into rectangular bricks, so that each brick contains only a single dipole. Figure 3 (a) shows the dipoles and Figure 3 (b) shows the bricks. Incident wave is a linearly polarized planewave propagating toward the negative z direction. The derivation of the methods does not set any requirements for the incident fields and, e.g., oblique incidence can be considered without any modifications to the algorithms. The detailed geometrical data is given in the second column of Table 1.

The scattering problem is formulated using the methods described in the previous sections and with the EFIE. The bricks are divided to $4 \times 4 \times 2$ small rectangles and each rectangle is divided into four triangles. The numbers of triangles and (interior) edges on the dipoles and brick's surface are shown in the second column of Table 1. The results are verified by solving the same problem with the conventional MoM using EFIE and 2700 RWGs. Figure 4 shows the monostatic RCS as a function of frequency. In the TEPA-CBFM, we consider the primary CBFs of the

bricks and all secondary ones, hence, the total number of CBFs for all frequencies is $25^2 = 625$. In the TEPA-CBFM-pw method, the planewave based CBFs are found by first using 360 initial planewave excitations from different directions. Then, SVD with the tolerance 10^{-3} is used to determine the most important directions that are used to generate the CBFs of the bricks. The total DoF in CBF-pw depends on the frequency and varies from 275 at 7 GHz (11 CBFs for each brick) to 425 at 17 GHz (17 CBFs for each brick).

In LEGO-EEM, the tolerance for defining the last coupled eigenvalue is set to 10^{-5}. Accordingly (see [14]), the expected accuracy of computed currents (over bricks) is no larger 10^{-2} (as the bricks are not adjacent). With this criterion, the number of coupled eigencurrents is 30 for each brick and the same for all frequencies. The total number of DoF in LEGO-EEM is thus 750.
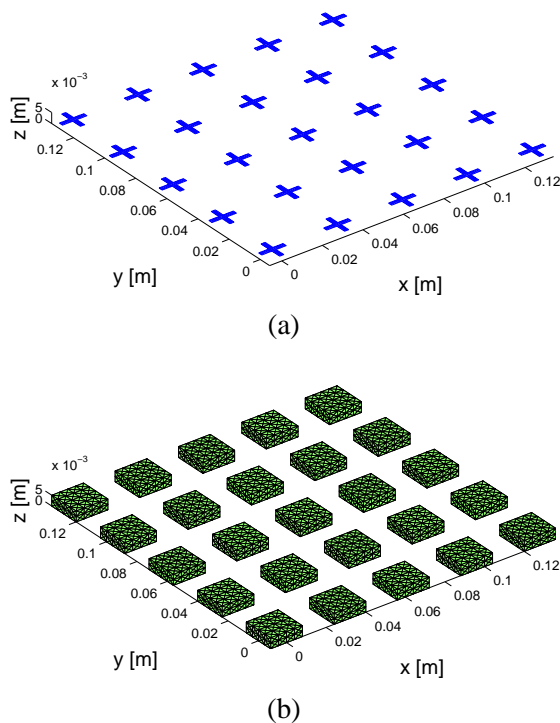

(a)

(b)

Fig. 3. An array of cross dipoles: (a) original structure (dipoles), (b) bricks.

As a second example, a larger problem is considered. We, also, study the effect of changing the size of the bricks. Consider a 5×5 array of double cross dipoles by putting two similar dipoles as used in the first example on the top of each other. The dipoles
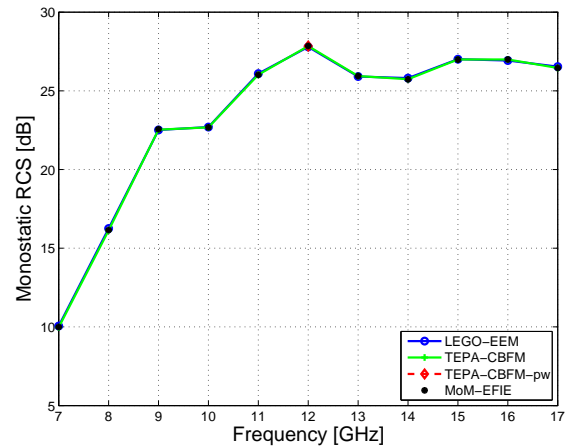

Fig. 4. Monostatic RCS in dB for the geometry of Figure 3 as a function of frequency.

are arranged in a similar regular lattice parallel to the xy plane as in the previous example. Figure 5 shows the geometry and discretization of a single element and Figure 6 shows the full geometry.
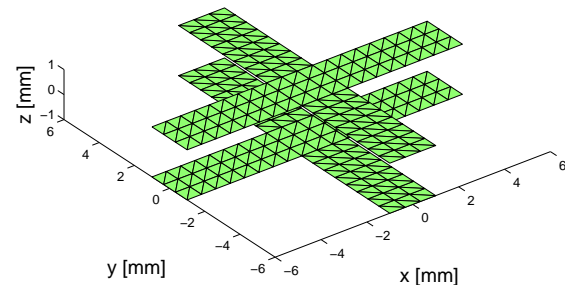

Fig. 5. A double cross dipole.

Figure 7 shows the monostatic RCS as a function of frequency. We have used two different brick sizes. The detailed geometrical data is given in the last two columns of table 1. The bricks are discretized so that first each face of a brick is divided into $4 \times 4 \times 2$ (first case) or $5 \times 5 \times 2$ (second case) planar rectangles and then each rectangle is divided into four triangles. A direct discretization of (16) with MoM (without CBFM and EEM) would lead to 19200 (first case) and 27000 (second case) unknowns, respectively.

Figure 8 shows the required DoF of the TEPA-CBFM-pw method. The CBFs are found using a similar procedure as in the first example. As the frequency or the brick size is increased, the number of required
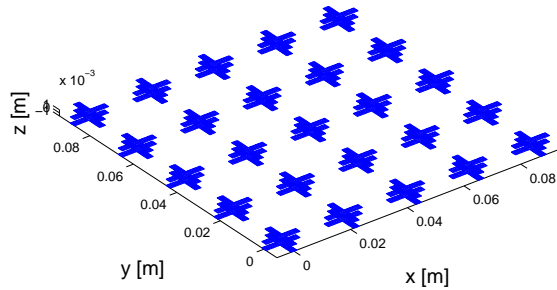
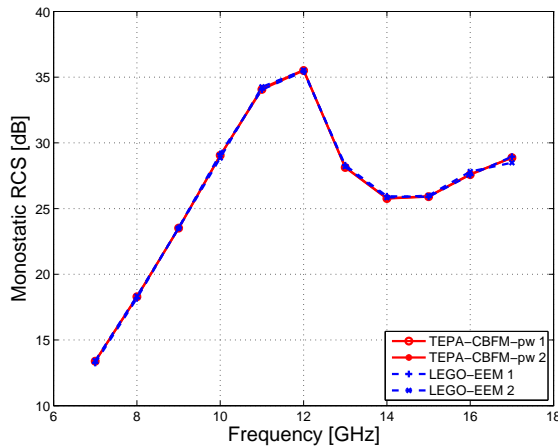Fig. 6. An array of double cross dipoles.

Fig. 7. Monostatic RCS in dB for the geometry of Figure 6 as a function of frequency for two brick sizes. 1 = brick size $16 \times 16 \times 4$mm and 2 = brick size $20 \times 20 \times 4$mm.

planewave based CBFs increases too. This can be explained by the facts that for higher frequencies, the current distribution on the bricks' surfaces become more complicated, and that as the bricks' distance becomes smaller, the coupling between the bricks becomes stronger. In this example, the CBFM based on the primary and secondary basis functions was not applied.

In LEGO-EEM, the DoF were set to $70 \times 25 = 1750$ and $100 \times 25 = 2500$ for the cases 1 and 2, respectively, 70 and 100 being the number of coupled eigencurrents contributed by each brick [4]. The tolerances for the coupled eigencurrents are 10^{-4} for the first case and 10^{-5} for the second one. As the spectrum of $\mathcal{S}_{ll}$ is insensitive to frequency to a large extent [14], the required number of DoF does not change with frequency either. On the other hand, the number of coupled eigencurrents is affected by both a brick's

size and the relative distance among the bricks modeling the structure. In case 2, the spectrum of $\mathcal{S}_{ll}$ decays faster than in case 1, because the brick's boundary is set farther away from the crosses. Nonetheless, since in case 2 the bricks are closer than in case 1, a stronger coupling is expected and, accordingly, more coupled eigencurrents are necessary. In the limiting case, when the bricks touch one another – which is the worst case scenario – a criterion has been developed to relate the error on the computed scattered currents (i.e., the near fields) to the number of coupled eigencurrents [14, 15]. Such a criterion can be used to control the error a priori. In situations when the bricks are separated (as discussed here), given that the coupling decreases with increasing bricks' distance, the aforesaid criterion most certainly yields a convenient upper bound to the error.
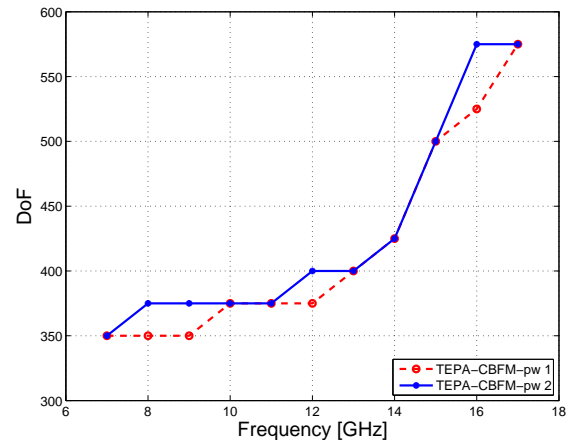

Fig. 8. The number of DoF of the TEPA-CBFM-pw as a function of frequency for two brick sizes.

VII. CONCLUSIONS

In this paper, two algorithms, the tangential equivalence principle algorithm (TEPA) [3] and the linear embedding via Green's operators (LEGO) [4], are reviewed for solving EM scattering problems. A general framework of the methods is presented and the methods are shown to be based on the same principles and operators. The major difference is on the form of the matrix equation to be solved. In addition, two macro basis function methods, the characteristic basis function method (CBFM) and the eigencurrent expansion method (EEM), are applied to reduce the number of unknowns. The developed hybrid methods, TEPA-CBFM and LEGO-EEM, are shown to lead to

dramatic reduction on the size of the matrix equation and hence, allow efficient solutions of large problems with reduced computer resources.

The numerical results show that the planewave based CBFM may be the most efficient method to reduce the number of degrees of freedom. However, the number of the required CBFs depends on the frequency, and the bricks' size and distance. In EEM, on the other hand, the number of degrees of freedom can be controlled a priori.

ACKNOWLEDGMENT

REFERENCES

[1] K. Zhao, V. Rawat, and J.-F. Lee, "A domain decomposition method for electromagnetic radiation and scattering analysis of multi-target problems," *IEEE Trans. Antennas Propag.*, vol. 56, no. 8, pp. 2211-2221, Aug. 2008.

[2] J.-M. Jin, Z. Lou, Y. J. Li, N. W. Riley, and D. J. Riley, "Finite element analysis of complex antennas and arrays," *IEEE Trans. Antennas Propag.*, vol. 56, no. 8, pp. 2211-2221, Aug. 2008.

[3] P. Ylä-Oijala and M. Taskinen, "Electromagnetic scattering by large and complex structures with surface equivalence principle algorithm," *Waves in Random and Complex Media*, vol. 19, no. 1, pp. 105-125, Feb. 2009.

[4] V. Lancellotti, B. P. de Hon, and A. G. Tijhuis, "An eigencurrent approach to the analysis of electrically large 3-D structures using linear embedding via Green's operators," *IEEE Trans. Antennas Propag.*, vol. 57, no. 11, Nov. 2009.

[5] M-K. Li and W. C. Chew, "Wave-field interaction with complex structures using equivalence principle algorithm," *IEEE Trans. Antennas Propag.*, vol. 55, no. 1, pp. 130-138, Jan. 2007.

[6] M.-K. Li, W. C. Chew, and L. J. Jiang, "A domain decomposition scheme based on equivalence theorem," *Microw. Optical Techn. Letters*, vol. 48, no. 9, pp. 1853-1857, Sep. 2006.

[7] M-K. Li and W. C. Chew, "Multiscale simulation of complex structures using equivalence principle algorithm with high-order field point sampling scheme," *IEEE Trans. Antennas Propag.*, vol. 56, no. 8, pp. 2389-2397, 2008.

[8] A. M. van de Water, B. P. de Hon, M. C. van Beurden, A. G. Tijhuis, and P. de Maagt, "Linear embedding via Green's operators: A modeling technique for finite electromagnetic band-gap structures," *Phys. Rev. E*, vol. 72, pp. 1-11, 2005.

[9] V. V. S. Prakash and R. Mittra, "Characteristic basis function method: A new technique for efficient solution of method of moments matrix equations," *Microw. Optical Techn. Letters*, vol. 36, no. 2, pp. 95-100, Jan. 2002.

[10] E. Lucente, A. Monorchio and R. Mittra, "An iteration-free MoM approach based on excitation independent characteristic basis functions for solving large multiscale electromagnetic problems," *IEEE Trans. Antennas Propag.*, vol. 56, no. 4, pp. 999-1007, April 2008.

[11] J. Laviada, M. R. Pino, and F. Las-Heras, "Characteristic spherical wave expansion with application to scattering and radiation problems," *IEEE Antennas and Wireless Propagation Letters*, vol.8, pp. 599-602, 2009.

[12] J. Laviada, F. Las-Heras, M. R. Pino, and R. Mittra, "Solution of electrically large problems with multilevel characteristic basis functions," *IEEE Trans. Antennas Propag.*, vol. 57, no. 10, pp. 3189-3198, Oct., 2009.

[13] R. Mittra, "Characteristic basis function method (CBFM) – An iterative-free domain decomposition approach in computationally electromagnetics," *ACES Journal*, vol. 24, no. 2, pp. 204-223, April 2009.

[14] V. Lancellotti, B. P. de Hon, and A. G. Tijhuis, "On the convergence of the eigencurrent expansion method applied to linear embedding via Green's operators (LEGO)," *IEEE Trans. Antennas Propag.*, vol. 58, no. 10, pp. 3231-3238, Oct. 2010.

[15] V. Lancellotti, B. P. de Hon, and A. G. Tijhuis, "A priori error estimate and control in the eigencurrent expansion method applied to linear embedding via Green's operators (LEGO)," *2010 IEEE International Symposium on Antennas and Propagation*, Toronto, Canada, July, 2010.